Gene to mouse atlas registration using a landmark-based nonlinear elasticity smoother

Tungyou Lin[a], Carole Le Guyader[c], Erh-Fang Lee[b], Ivo D. Dinov[b], Paul M. Thompson[b], Arthur W. Toga[b], and Luminita A. Vese[a]

[a]Department of Mathematics, UCLA, Los Angeles, U.S.A.
[b]Laboratory of Neuro Imaging, UCLA School of Medicine, Los Angeles, U.S.A.
[c]IRMAR, UMR CNRS 6625, Institut National des Sciences Appliquées de Rennes, France

ABSTRACT

We propose a unified variational approach for registration of gene expression data to neuroanatomical mouse atlas in two dimensions. The proposed energy (minimized in the unknown displacement $\mathbf{u}$) is composed of three terms: a standard data fidelity term based on L^2 similarity measure, a regularizing term based on nonlinear elasticity (allowing larger smooth deformations), and a geometric penalty constraint for landmark matching. We overcome the difficulty of minimizing the nonlinear elasticity functional by introducing an auxiliary variable $\mathbf{v}$ that approximates $\nabla\mathbf{u}$, the Jacobian of the unknown displacement $\mathbf{u}$. We therefore minimize now the functional with respect to the unknowns $\mathbf{u}$ (a vector-valued function of two dimensions) and $\mathbf{v}$ (a two-by-two matrix-valued function). An additional quadratic term is added, to insure good agreement between $\mathbf{v}$ and $\nabla\mathbf{u}$. In this way, the nonlinearity in the derivatives of the unknown $\mathbf{u}$ no longer exists in the obtained Euler-Lagrange equations, producing simpler implementations. Several satisfactory experimental results show that gene expression data are mapped to a mouse atlas with good landmark matching and smooth deformation. We also present comparisons with the biharmonic regularization. An advantage of the proposed nonlinear elasticity model is that usually no numerical correction such as regridding is necessary to keep the deformation smooth, while unifying the data fidelity term, regularization term, and landmark constraints in a single minimization approach.

Keywords: mouse atlas, gene expression, registration, nonlinear elasticity, landmarks, functional minimization, mutual information.

1. INTRODUCTION

An important task in medical imaging, for clinical studies of disease and for atlas-based identification and segmentation of anatomical structures, is to compare a subject/time variant template image T with an unbiased, reference image R. This is commonly done using image registration. Given a reference R and a template T, defined on image domain Ω, we want to find a smooth, invertible transformation to map T into an image *similar* to R. For images of the same modality, a well-registered template has geometric features and intensity distribution matched with the reference; for images produced by different mechanism and possessing distinct modalities, the goal of registration is to correlate the images while maintaining the modality of the template. In the case of mapping gene expression data to atlas, we want to match anatomically or geometrically significant points for the template with those corresponding ones for the reference.

Further author information (send correspondence to T.L.):
T.L.: E-mail: tungyoul@math.ucla.edu
C.L.G.: E-mail: cleguyad@insa-rennes.fr
I.D.D.: E-mail: ivo.dinov@loni.ucla.edu
P.M.T.: E-mail: thompson@loni.ucla.edu
A.W.T.: E-mail: toga@loni.ucla.edu
L.A.V.: E-mail: lvese@math.ucla.edu

Medical Imaging 2009: Image Processing, edited by Josien P. W. Pluim, Benoit M. Dawant,
Proc. of SPIE Vol. 7259, 72592Q · © 2009 SPIE
CCC code: 1605-7422/09/$18 · doi: 10.1117/12.812491

1.1 Prior Related Work

An extensive overview of registration models is presented in[1] including parametric models such as landmark-based spline registration, and nonparametric models employing linear diffusion, linear elasticity, biharmonic ("curvature") and fluid regularizations . Also, variational methods for regularization of the deformation, by linear elasticity or by diffusion tensor, using mutual information and other information-theoretic approaches, are presented in[2] in a theoretical framework.

For models that deal with larger deformations, we refer to[3] for a well-known large deformation fluid registration method (not in variational form), and to a variational registration for large deformations (LDDMM),[4,5] The log-unbiased fluid registration method,[6,7] developed more recently also handles large deformations. Besides fluid models, nonlinear elasticity regularization is implemented using the finite element method in[8] and.[9] Non-linear elasticity principles have also been used with the regularized gradient flow in.[10]

As for landmark-based registration methods, we refer to[11] where a consistent landmark and intensity-based registration method is presented using thin-plate spline regularization (or biharmonic regularization). Another related reference is[12] where data fidelity, spline regularization and soft landmark constraints are combined, as in the present work.

1.2 Our Approach

There are forward and backward registrations. The former is done in the Lagrangian framework where a forward transformation Ψ is sought and grid points x with intensity values $T(x)$ are moved and arrive at non-grid points y with intensity values $T(\Psi^{-1}(y)) = T(x),\ \forall x \in \Omega$ or $\forall y \in \Psi(\Omega)$. In this work, we adopt the Eulerian framework to find a backward transformation $\Phi = \Psi^{-1}$ such that grid points y in the deformed image arrive from non-grid points $x = \Phi(y)$ and are assigned with intensity values $T(x) = T(\Phi(y))$. For more detailed description of the two frameworks, readers may refer to.[1]

For data fidelity, we minimize the L^2 distance of the pixel by pixel intensity values between $T \circ \Phi$ and R (although our data, mouse gene expression and mouse atlas, come from different modalities, we show that the L^2 measure is satisfactory without employing more complicated information theoretic measures, such as the mutual information; in our calculations, we show numerically that minimizing the L^2 distance, increases the mutual information with iterations). The mapping of landmark points is done simply by minimizing the sum of the squared distances between the points without incorporating any spline model. We propose a nonlinear elasticity model for regularization of the displacement vector field, since this allows smooth larger deformations and thus will work without the need for regridding most of the time. In prior work based on nonlinear elasticity principles, the finite element method has been used. To have a simpler numerical algorithm, we hereby introduce an auxiliary variable for the Jacobian matrix of the displacement in order to remove the nonlinearity in the derivatives of the displacement vector field. This idea has been inspired from a more theoretical work[13] and by the prior work[14] for a joint segmentation and registration model. The present manuscript is a continuation of very preliminary work reported in.[15]

1.3 Motivation for Mapping Mouse Gene Expression Data to Mouse Atlas

The C57BL/6J mouse digital brain atlas,[16,17] is a comprehensive framework for storing and accessing information, and serves as a canonical representation of the mouse brain. We use the mouse brain atlas as a common and unbiased framework and map gene expression data to the atlas in order to facilitate the integration of anatomic, genetic, and physiologic observations from multiple subjects in a common space. Since genetic mutations and knock-out strains of mice provide critical models for a variety of human diseases, such linkage between genetic information and anatomical structure is important.

2. DESCRIPTION OF THE PROPOSED REGISTRATION MODELS

Let Ω be a bounded, open and connected subset of the plane. In the present work, we consider two-dimensional images only, however the proposed framework can easily be extended to volumetric data. Denote by R the reference image and by T the template image. We want to find a smooth transformation $\Phi(\mathbf{x}) = \mathbf{x} + \mathbf{u}(\mathbf{x}),\ \mathbf{x} =$

(x_1, x_2) that minimizes an energy functional consisting of data fidelity, landmark constraints, and regularization. The general form of such functional is as follows,

$$\inf_{\mathbf{u}} \Big\{ J(\mathbf{u}) = Fid_{T,R}(\mathbf{u}) + \gamma D^{LM}(\mathbf{u}) + \alpha Reg(\mathbf{u}) \Big\},$$

where γ and α are positive parameters chosen based on the images. By gradient descent, we solve the time-dependent Euler-Lagrange equation in the displacement vector field $\mathbf{u} = (u_1, u_2)$, instead of directly in Φ:

$$\frac{\partial u_l}{\partial t} = -\frac{\partial Fid(\mathbf{u})}{\partial u_l} - \gamma \frac{\partial D^{LM}(\mathbf{u})}{\partial u_l} - \alpha \frac{\partial Reg(\mathbf{u})}{\partial u_l},\ l = 1, 2.$$

2.1 L^2 Data Fidelity in Eulerian Framework

We have chosen the standard L^2 distance as dissimilarity measure between $T \circ \Phi$ and R, and this is complemented by the use of additional landmarks as geometrical constraints. We minimize the L^2 distance function

$$Fid(\mathbf{u}) = \frac{1}{2} \int_{\Omega} |T(\mathbf{x} + \mathbf{u}(\mathbf{x})) - R(\mathbf{x})|^2 d\mathbf{x}$$

by computing its Gâteaux derivative

$$\frac{\partial Fid(\mathbf{u})}{\partial u_l} = (T(\mathbf{x} + \mathbf{u}(\mathbf{x})) - R(\mathbf{x}))T_{x_l}(\mathbf{x} + \mathbf{u}(\mathbf{x})),\ l = 1, 2$$

where T_{x_l} denotes the derivative of the intensity field of the template in the direction x_l, $l = 1, 2$.

2.2 Landmark Constraints

Let $\mathbf{x}^{R,k}$ be manually-selected landmark points for the reference R, and $\mathbf{x}^{T,k}$ those for the template T. We want to map $\mathbf{x}^{R,k}$ to $\mathbf{x}^{T,k}$ by a smooth deformation Φ such that $\Phi(\mathbf{x}^{R,k}) \sim \mathbf{x}^{T,k}$ by minimizing the following landmark distance function:

$$D^{LM}(\mathbf{u}) = \frac{1}{2} \sum_{k=1}^{m} \|\mathbf{x}^{T,k} - \Phi(\mathbf{x}^{R,k})\|^2$$

where $\Phi(\mathbf{x}^{R,k}) = \mathbf{x}^{R,k} + \mathbf{u}(\mathbf{x}^{R,k})$. Then the Gâteaux derivative in u_1, u_2 are

$$\frac{\partial D^{LM}(\mathbf{u})}{\partial \mathbf{u}}(\mathbf{x}) = \begin{cases} -\Big(\mathbf{x}^{T,k} - \mathbf{x} - \mathbf{u}(\mathbf{x})\Big) & \text{if } \mathbf{x} = \mathbf{x}^{R,k} \\ 0 \quad \text{otherwise} \end{cases},$$

$k = 1, ..., m$ (m representing the number of landmarks).

2.3 Regularization

Viewing the shape change of the image after transformation as the deformation of an elastic material under external forces was first adopted by[18] in developing linear elastic registration method. Since the linear model works well for small deformations only, we propose a nonlinear elastic model to allow large deformations. Among the various nonlinear elastic models, we have chosen the St. Venant-Kirchhoff material for its simplicity.[19] Compared with linear registration models, the proposed nonlinear elasticity smoother allows larger and smoother deformations without numerical correction (such as regridding[3]) most of the time. Since the nonlinear term has resulted in complicated nonlinear Euler-Lagrange equations, more difficult to discretize in practice, we propose a particular implementation that removes the non-linearity in the derivatives,[13].[14]

2.3.1 Proposed Nonlinear Elasticity Regularization

It is physically motivated to view the displacement of vector fields as the deformation of some material under external forces. The strain energy corresponding to Saint Venant-Kirchhoff hyperelastic materials[20] is given by $Reg(\mathbf{u}) = \int_\Omega W(\epsilon) d\mathbf{x}$, with tensor $\epsilon(\mathbf{u}) = \frac{1}{2}(\nabla \mathbf{u}^t + \nabla \mathbf{u} + \nabla \mathbf{u}^t \nabla \mathbf{u})$ and the stored energy $W(\epsilon) = \frac{\lambda}{2}(\text{trace}(\epsilon))^2 + \mu \text{trace}(\epsilon^2)$, where λ and μ are the Lamé coefficients of the material. Note that, by removing the nonlinear term $\nabla \mathbf{u}^t \nabla \mathbf{u}$, we obtain the linear elasticity regularization which allows small deformations only. To allow larger deformations, we keep the nonlinear term and the regularization is as follows:

$$Reg(\mathbf{u}) = \frac{\lambda}{8}\Big(2(\text{div}\mathbf{u}) + \sum_{k=1}^{2} |\nabla u_k|^2\Big)^2 + \frac{\mu}{4}\Big(\sum_{i=1}^{2}\Big[2\frac{\partial u_i}{\partial x_i} + \sum_{k=1}^{2}(\frac{\partial u_k}{\partial x_i})^2\Big]^2 + \sum_{i,j=1, i\neq j}^{2}\Big[\frac{\partial u_j}{\partial x_i} + \frac{\partial u_i}{\partial x_j} + \sum_{k=1}^{2}\frac{\partial u_k}{\partial x_i}\frac{\partial u_k}{\partial x_j}\Big]^2\Big).$$

It is cumbersome to directly compute and discretize its Gâteaux derivative in $\mathbf{u}$. To avoid this difficulty, we introduce in two dimensions the variable $\mathbf{v} = \begin{pmatrix} v_{11} & v_{12} \\ v_{21} & v_{22} \end{pmatrix}$, which approximates $\nabla \mathbf{u}$. For β large enough, $Reg(\mathbf{u})$ can be well approximated by

$$\begin{aligned} Reg_\beta(\mathbf{u}, \mathbf{v}) &= \int_\Omega \Big[W\Big(\frac{1}{2}(\mathbf{v}^t + \mathbf{v} + \mathbf{v}^t\mathbf{v})\Big) + \beta\|\mathbf{v} - \nabla\mathbf{u}\|_F^2\Big] d\mathbf{x} = \int_\Omega \Big(\frac{\lambda}{8}[2(v_{11}+v_{22}) + (v_{11}^2 + v_{12}^2 + v_{21}^2 + v_{22}^2)]^2 \\ &+ \frac{\mu}{4}[(2v_{11} + v_{11}^2 + v_{21}^2)^2 + (2v_{22} + v_{12}^2 + v_{22}^2)^2 + 2(v_{12} + v_{21} + v_{11}v_{12} + v_{21}v_{22})^2]\Big) d\mathbf{x} \\ &+ \beta \int_\Omega \Big[\Big|v_{11} - \frac{\partial u_1}{\partial x_1}\Big|^2 + \Big|v_{12} - \frac{\partial u_1}{\partial x_2}\Big|^2 + \Big|v_{21} - \frac{\partial u_2}{\partial x_1}\Big|^2 + \Big|v_{22} - \frac{\partial u_2}{\partial x_2}\Big|^2\Big] d\mathbf{x}, \end{aligned}$$

where $\|\cdot\|_F$ denotes the Frobenius norm.

Now, we solve by gradient descent the linearized Euler-Lagrange equations in u_l, $l = 1, 2$:

$$\frac{\partial u_l}{\partial t} = -(T(\mathbf{x} + \mathbf{u}(\mathbf{x})) - R(\mathbf{x}))T_{x_l}(\mathbf{x} + \mathbf{u}(\mathbf{x})) - \gamma \frac{\partial D^{LM}(\mathbf{u})}{\partial t}(\mathbf{x}) + 2\alpha\beta(\triangle u_l - \frac{\partial v_{l1}}{\partial x_1} - \frac{\partial v_{l2}}{\partial x_2}),\ l = 1, 2,$$

and we update the approximation matrix $\mathbf{v}$ by solving the four Euler-Lagrange equations in $\mathbf{v}$:

$$\begin{aligned} \frac{\partial v_{11}}{\partial t} &= 2\alpha\beta(\frac{\partial u_1}{\partial x_1} - v_{11}) - \alpha\lambda I(1 + v_{11}) - \alpha\mu(2v_{11} + v_{11}^2 + v_{21}^2)(1 + v_{11}) - \alpha\mu J v_{12}, \\ \frac{\partial v_{12}}{\partial t} &= 2\alpha\beta(\frac{\partial u_1}{\partial x_2} - v_{12}) - \alpha\lambda I v_{12} - \alpha\mu(2v_{22} + v_{12}^2 + v_{22}^2)v_{12} - \alpha\mu J(1 + v_{11}), \\ \frac{\partial v_{21}}{\partial t} &= 2\alpha\beta(\frac{\partial u_2}{\partial x_1} - v_{21}) - \alpha\lambda I v_{21} - \alpha\mu(2v_{11} + v_{11}^2 + v_{21}^2)v_{21} - \alpha\mu J(1 + v_{22}), \\ \frac{\partial v_{22}}{\partial t} &= 2\alpha\beta(\frac{\partial u_2}{\partial x_2} - v_{22}) - \alpha\lambda I(1 + v_{22}) - \alpha\mu(2v_{22} + v_{12}^2 + v_{22}^2)(1 + v_{22}) - \alpha\mu J v_{21}, \end{aligned}$$

where $I = v_{11} + v_{22} + \frac{1}{2}v_{11}^2 + \frac{1}{2}v_{21}^2 + \frac{1}{2}v_{12}^2 + \frac{1}{2}v_{22}^2$, and $J = v_{12} + v_{21} + v_{11}v_{12} + v_{21}v_{22}$. The following are the semi-implicit finite difference schemes for the time-dependent Euler-Lagrange equations for the regularization term in $\mathbf{u}$ and in $\mathbf{v}$:

$$\begin{aligned} &\frac{{u_l}_{i,j}^{n+1} - {u_l}_{i,j}^{n}}{\triangle t} = -(T(\mathbf{x}_{i,j} + \mathbf{u}^n(\mathbf{x}_{i,j})) - R(\mathbf{x}_{i,j}))T_{x_l}(\mathbf{x}_{i,j} + \mathbf{u}^n(\mathbf{x}_{i,j})) - \gamma\frac{\partial D^{LM}(\mathbf{u}^n)}{\partial t}(\mathbf{x}_{i,j}) \\ + \quad &2\alpha\beta\Big(\frac{{u_l}_{i+1,j}^{n} - 2{u_l}_{i,j}^{n+1} + {u_l}_{i-1,j}^{n}}{h^2} + \frac{{u_l}_{i,j+1}^{n} - 2{u_l}_{i,j}^{n+1} + {u_l}_{i,j-1}^{n}}{h^2} - \frac{{v_{l1}}_{i+1,j}^{n} - {v_{l1}}_{i-1,j}^{n} + {v_{l2}}_{i,j+1}^{n} - {v_{l2}}_{i,j-1}^{n}}{2h}\Big), \end{aligned}$$

and

$$\frac{v_{11}^{n+1} - v_{11}^{n}}{\triangle t} = 2\beta(\frac{\partial u_1^n}{\partial x_1} - v_{11}^{n+1}) - (\lambda E_1 E_5 + \mu(E_2 E_5 + E_3 v_{12})),$$

$$\begin{aligned}
\frac{v_{12}^{n+1}-v_{12}^{n}}{\triangle t} &= 2\beta(\frac{\partial u_1^n}{\partial x_2}-v_{12}^{n+1})-(\lambda E_1 v_{12}+\mu(E_4 v_{12}+E_3 E_5)),\\
\frac{v_{21}^{n+1}-v_{21}^{n}}{\triangle t} &= 2\beta(\frac{\partial u_2^n}{\partial x_1}-v_{21}^{n+1})-(\lambda E_1 v_{21}+\mu(E_2 v_{21}+E_3 E_6)),\\
\frac{v_{22}^{n+1}-v_{22}^{n}}{\triangle t} &= 2\beta(\frac{\partial u_2^n}{\partial x_2}-v_{22}^{n+1})-(\lambda E_1 E_6+\mu(E_4 E_6+E_3 v_{21})),
\end{aligned}$$

where

$$E_1 = v_{11}+\tfrac{1}{2}v_{11}^2+\tfrac{1}{2}v_{21}^2+v_{22}+\tfrac{1}{2}v_{12}^2+\tfrac{1}{2}v_{22}^2,\quad E_2 = 2v_{11}+v_{11}^2+v_{21}^2,\quad E_3 = 2v_{22}+v_{12}^2+v_{22}^2,$$
$$E_4 = v_{12}+v_{21}+v_{11}v_{12}+v_{21}v_{22},\quad E_5 = 1+v_{11},\quad E_6 = 1+v_{22}.$$

2.3.2 Biharmonic Regularization

For comparison purposes, we also consider the biharmonic regularization (so-called curvature regularization),[1] defined as

$$Reg(\mathbf{u}) = \frac{1}{2}\sum_{l=1}^{2}\int_{\Omega}(\triangle u_l)^2 d\mathbf{x}.$$

The Laplacian term $\triangle u_l$ approximates the curvature of level lines of u_l, thus we could say that this regularizer minimizes the curvature of the displacement vectors.[1] According to,[1] among the nonlinear methods, the biharmonic registration is less dependent on the initial position of the image and thus is more suitable when an affine linear pre-registration is not available. The time-dependent Euler-Lagrange equations are the following:

$$\frac{\partial \mathbf{u}}{\partial t} = -(T(\mathbf{x}+\mathbf{u}(\mathbf{x}))-R(\mathbf{x}))T_{x_l}(\mathbf{x}+\mathbf{u}(\mathbf{x}))-\gamma\frac{\partial D^{LM}(\mathbf{u})}{\partial t}(\mathbf{x})-\alpha\triangle^2\mathbf{u},\ l=1,2.$$

The semi-implicit finite difference scheme that we adopted is as follows (different from the implementation presented in[1]):

$$\begin{aligned}
\frac{u_{l_{i,j}}^{n+1}-u_{l_{i,j}}^{n}}{\triangle t} &= -(T(\mathbf{x}_{i,j}+\mathbf{u}^n(\mathbf{x}_{i,j}))-R(\mathbf{x}_{i,j}))T_{x_l}(\mathbf{x}_{i,j}+\mathbf{u}^n(\mathbf{x}_{i,j}))-\gamma\frac{\partial D^{LM}(\mathbf{u}^n)}{\partial t}(\mathbf{x}_{i,j})-\alpha\frac{1}{h^4}(16u_{l_{i,j}}^{n+1}\\
&+ u_{l_{i+2,j}}^{n}-6u_{l_{i+1,j}}^{n}-6u_{l_{i-1,j}}^{n}+u_{l_{i-2,j}}^{n}+u_{l_{i,j+2}}^{n}-6u_{l_{i,j+1}}^{n}-6u_{l_{i,j-1}}^{n}+u_{l_{i,j-2}}^{n}\\
&+ u_{l_{i+1,j+1}}^{n}+u_{l_{i+1,j-1}}^{n}+u_{l_{i-1,j+1}}^{n}+u_{l_{i-1,j-1}}^{n}),\ l=1,2.
\end{aligned}$$

3. EXPERIMENTAL RESULTS

Numerical Correction: Regridding An admissible deformation field $\Phi:\overline{\Omega}\to\overline{\Omega}$, $\Phi(\mathbf{x})=\mathbf{x}+\mathbf{u}(\mathbf{x})$, should satisfy $det(\nabla\Phi)>0$ in Ω, $\Phi(\mathbf{x})=\mathbf{x}$ on $\partial\Omega$, and Φ is one-to-one and onto on $\overline{\Omega}$. To enforce such a constraint, some numerical corrections such as regridding are introduced, as in.[3] In present work, if $det(\nabla(\Phi)^{n+1})<tol$ (here $tol=0.025$), we set the displacement field $\mathbf{u}^{n+1}=0$, the new intermediate template $T(\mathbf{x})=T(\mathbf{x}+\mathbf{u}^n)$, and the new reference landmarks $\mathbf{x}^{R,k}=\mathbf{x}^{T,k}-\mathbf{u}^n(\mathbf{x}^{R,k})$. After the iterations, we calculate the composite displacement field by interpolating each intermediate displacement field, which is saved during the regridding process, based on its succeeding one. The algorithm is given as follows:

(1) formulate identity matrices S_1 and S_2 so that $S_1(x,y)=x$, $S_2(x,y)=y$;
initialize $\mathbf{u}^n=(u_1^n,u_2^n)$;
(2) iteration starts: compute $\mathbf{u}^{n+1}$;
update matrices S_{11} and S_{22} so that $S_{11}^{n+1}=S_1+u_1^{n+1}$, $S_{22}^{n+1}=S_2+u_2^{n+1}$;
if $det(Jacobian(\Phi))<tol$,
then $regrid.count=regrid.count+1$;
$T(\cdot)=T(\cdot+\mathbf{u}^n(\cdot))$;
$\mathbf{u}^{n+1}=\mathbf{u}^n$;
save $\mathbf{u}^n$ as data files $u_k(regrid.count)$, $k=1,2$;

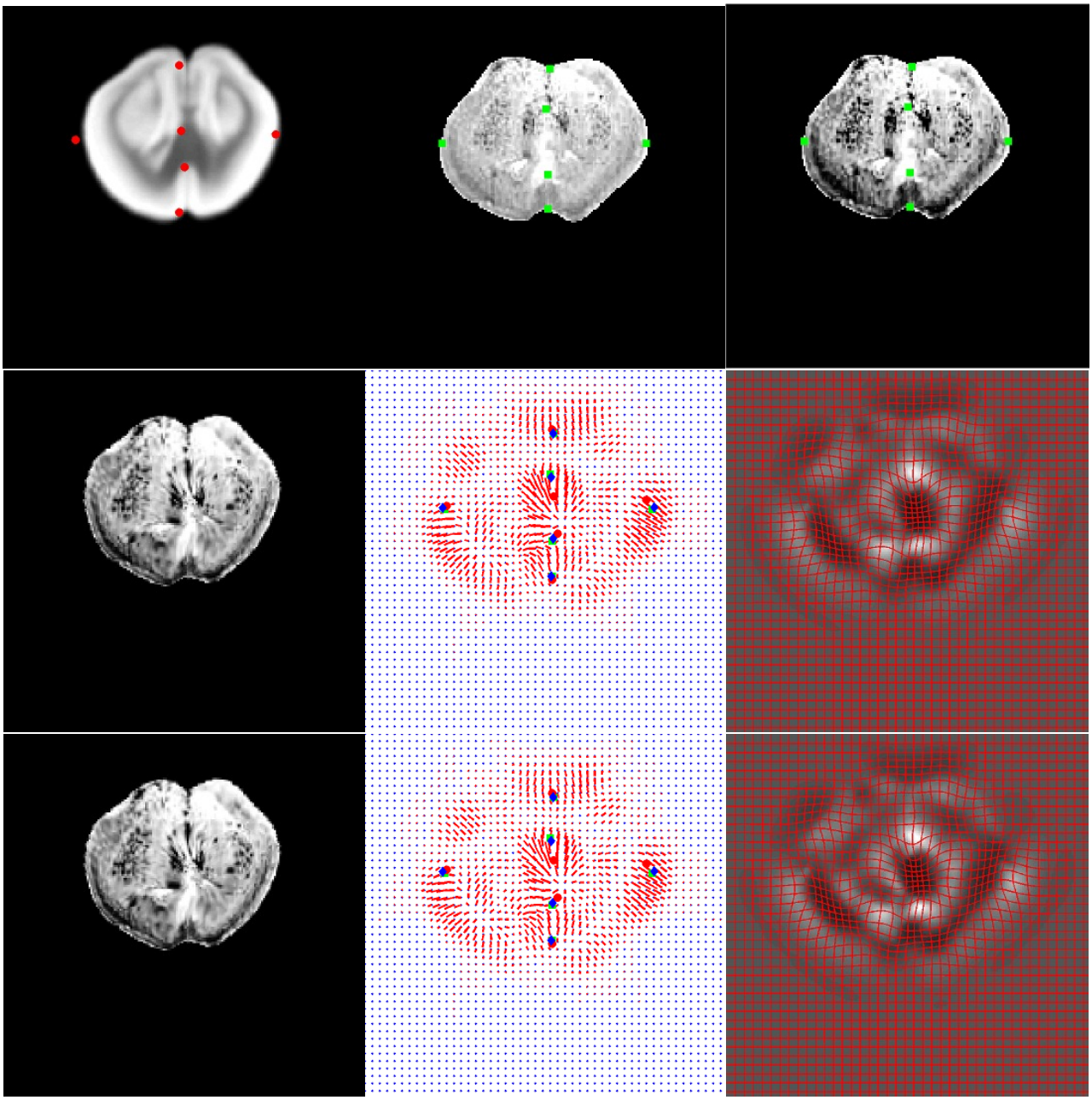

Figure 1. Pair 1: mouse atlas (reference R), gene expression (template T), and gene expression after histogram equalization with specified landmarks (top, left to right); deformed template, deformation field and landmarks transformation, $1/det(\nabla\Phi)$ and deformed grid using BH regularization (middle, left to right), and those using NE regularization (bottom, left to right.)

end;

(3) iteration ends:

if $regrid.count > 0$

then composite.$S_{kk} = S_{kk}^{final.iteration}$;

composite.$u_k = u_k^{final.iteration}$, $k = 1, 2$;

for $i = regrid.count : -1 : 1$

read and load data files $u_k(regrid.count)$;

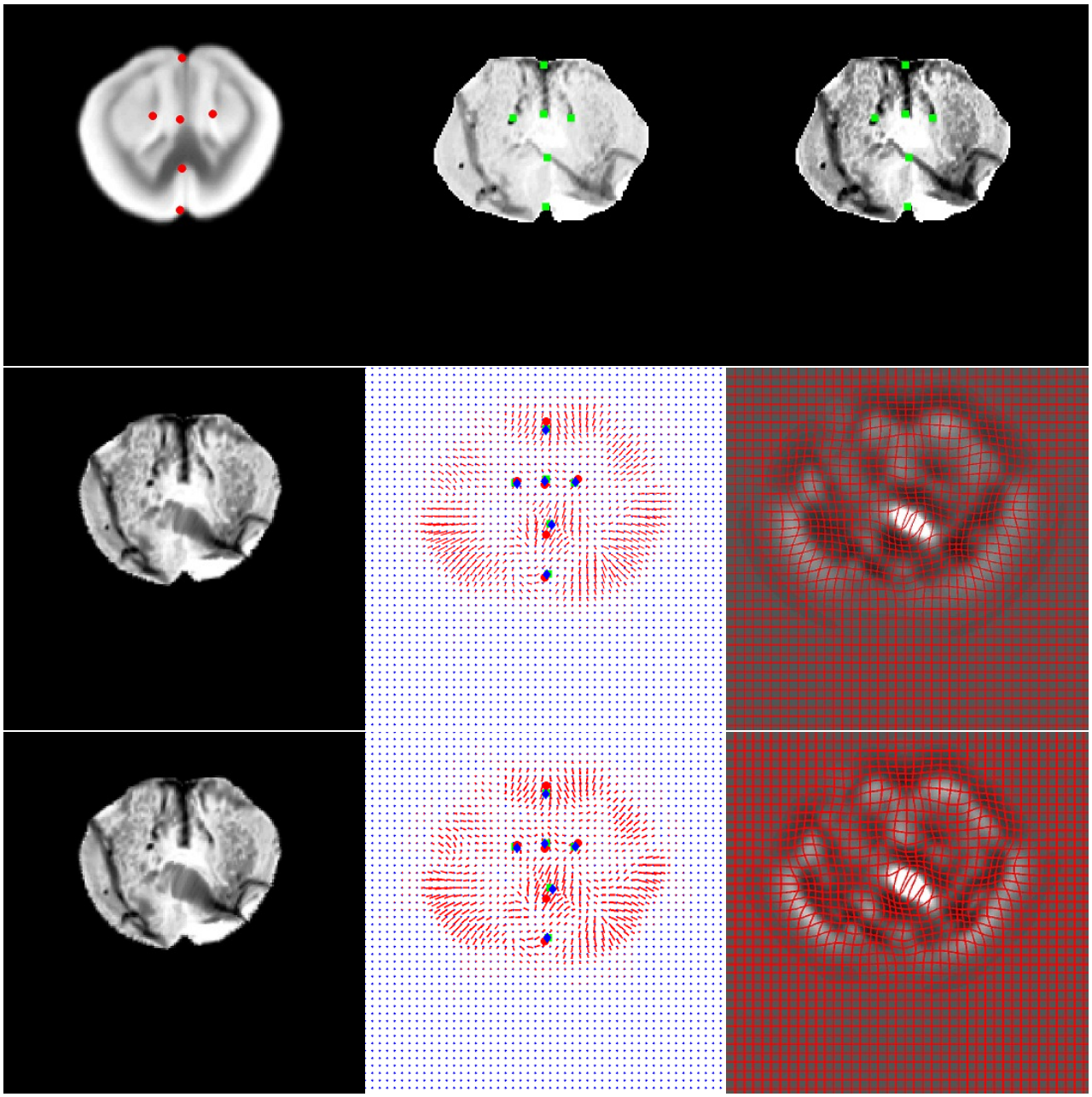

Figure 2. Pair 2: mouse atlas (reference R), gene expression (template T), and gene expression after histogram equalization with specified landmarks (top, left to right); deformed template, deformation field and landmarks transformation, $1/det(\nabla\Phi)$ and deformed grid using BH regularization (middle, left to right), and those using NE regularization (bottom, left to right.)

$U0_k$=$u_k(regrid.count)$, $k = 1, 2$;
composite.$u_k(regrid.count)$=composite.$u_k(regrid.count)$
+interpolation($U0_k$,composite.S_{22},composite.S_{11});
composite.$S_{kk}(regrid.count)$=S_k+composite.$u_k(regrid.count)$;
end
u_k=composite.$u_k(1)$;
S_{kk}=composite.S_{kk}.

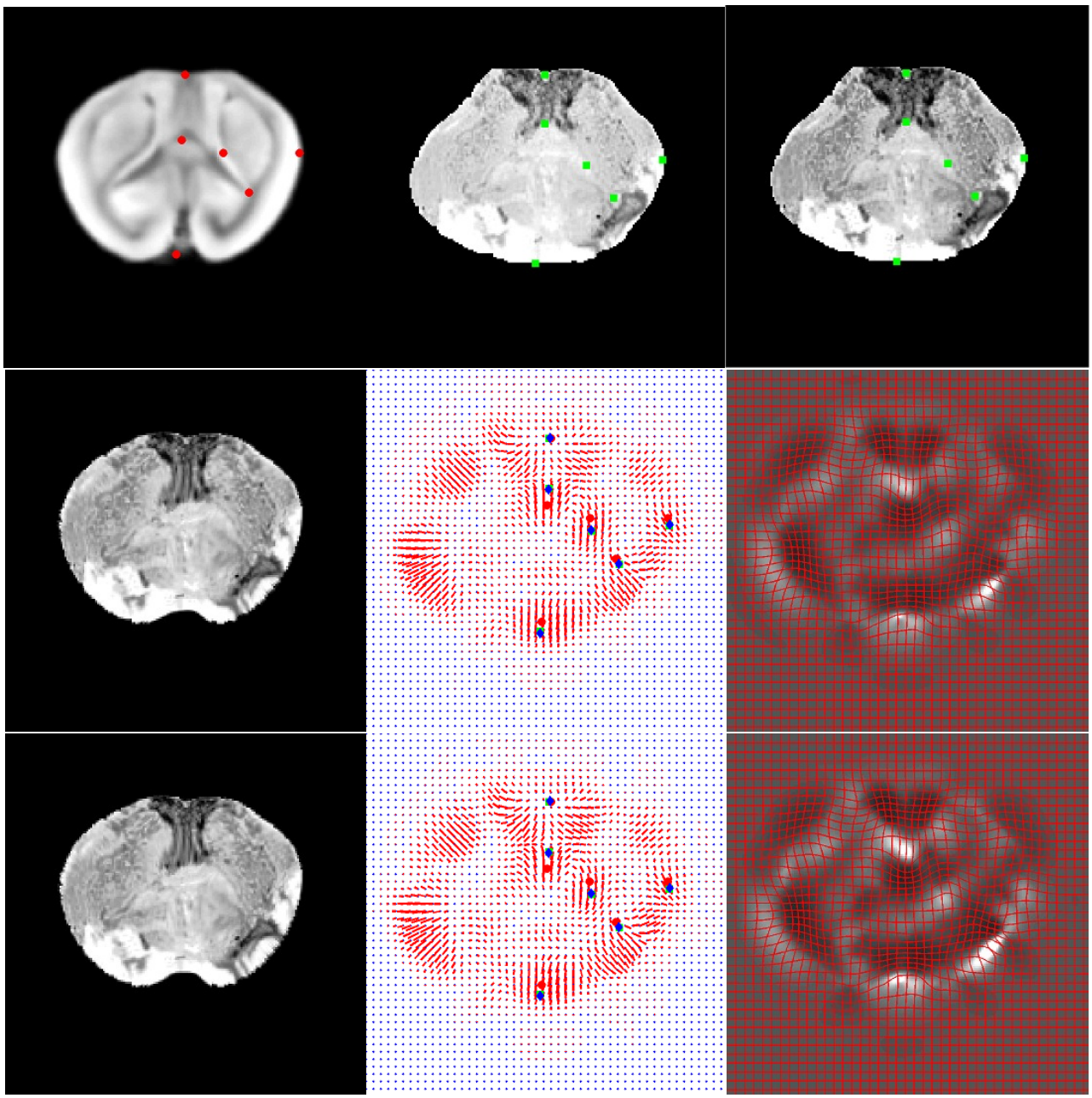

Figure 3. Pair 3: mouse atlas (reference R), gene expression (template T), and gene expression after histogram equalization with specified landmarks (top, left to right); deformed template, deformation and landmarks transformation, $1/det(\nabla\Phi)$ and deformed grid using BH regularization (middle, left to right), and those using NE regularization (bottom, left to right.)

Note that models requiring fewer regridding steps are considered better since a well-defined transformation is desired. The following results are obtained mostly without regridding.

Registration Results of Mouse Gene Expression to Mouse Atlas We show now experimental results obtained by the two methods presented in the previous section for mapping a 2D slice of mouse brain gene expression data (template T) to its corresponding 2D slice of the mouse brain atlas (reference R), in the presence of landmarks, and for 8 such data pairs (T, R). The data is provided by the Center for Computational Biology,

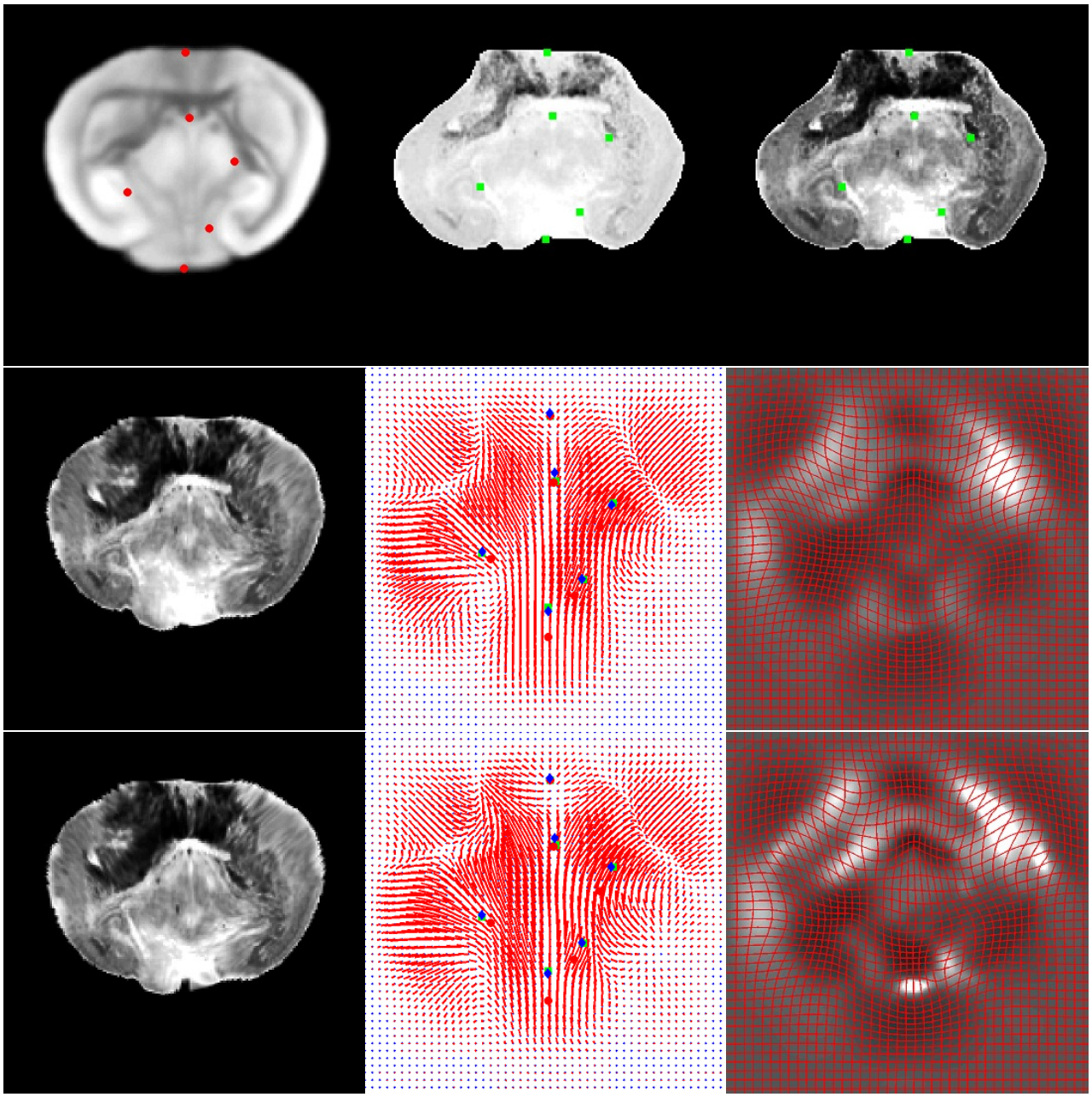

Figure 4. Pair 4: mouse atlas (reference R), gene expression (template T), and gene expression after histogram equalization with specified landmarks (top, left to right); deformed template, deformation field and landmarks transformation, $1/det(\nabla\Phi)$ and deformed grid using BH regularization (middle, left to right), and those using NE regularization (bottom, left to right.)

UCLA. The mouse atlas acquired from the LONI database was pre-segmented. The gene expression data was segmented manually to facilitate data processing in other applications. Some studies have developed algorithms for automatically segmenting the brain area of gene expression data. Moreover, since the reference and template come from different modalities, and that the intensity variation of the gene expression data in the non-background region is so small (the gene expression images almost resemble to piecewise-constant images), we also match the histogram of the gene expression data to that of the atlas before registration, in order to facilitate better registration for area away from the edges. The two models have been independently tested on 8 pairs, all of size

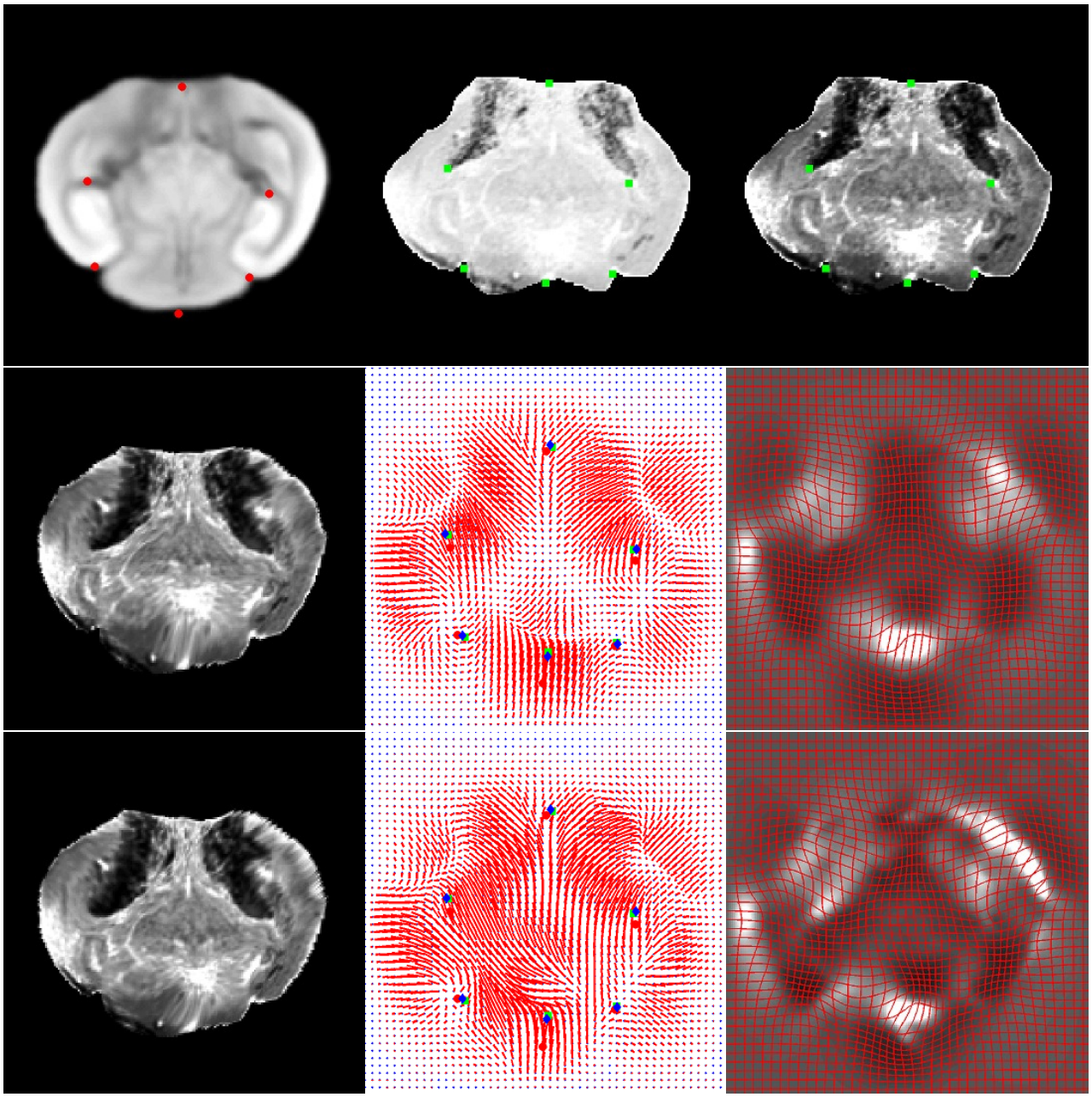

Figure 5. Pair 5: mouse atlas (reference R), gene expression (template T), and gene expression after histogram equalization with specified landmarks (top, left to right); deformed template, deformation field and landmarks transformation, $1/det(\nabla\Phi)$ and deformed grid using BH regularization (middle, left to right), and those using NE regularization (bottom, left to right.)

200x200 pixels. The non-brain regions have been removed and set to zero, to produce better matching. The landmarks are marked by an experienced neuroanatomist based on the anatomical structures present in images. This is based on prior knowledge in neuroanatomy. The number of iterations for both methods depends on how small we wish the landmark distance and the similarity measure to be.

Figures 1-8 are registration results of the eight pairs of images after the same number of iterations for both models. Each figure contains (1) a reference-template (before and after histogram equalization) data pair with landmark points marked, (2) the deformed template, distortion map with landmark points marked, and (3)

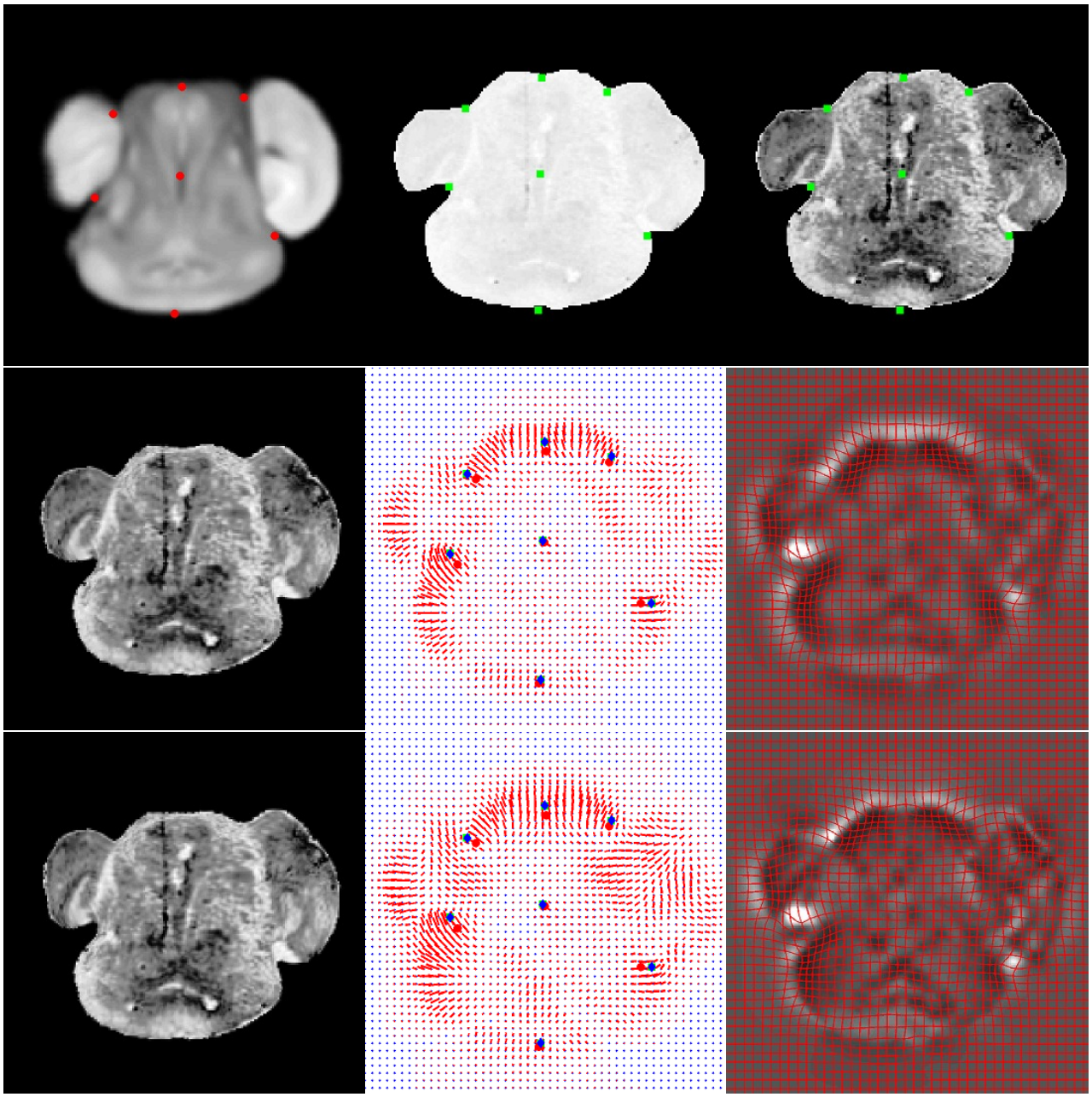

Figure 6. Pair 6: mouse atlas (reference R), gene expression (template T), and gene expression after histogram equalization with specified landmarks (top, left to right); deformed template, deformation field and landmarks transformation, $1/det(\nabla\Phi)$ and deformed grid using BH regularization (middle, left to right), and those using NE regularization (bottom, left to right.)

inverse of the determinant of Jacobian of Φ with deformed grid. The distortion maps draw the vectors from the grid points of the reference image to the non-grid points after registration; the original reference/template landmarks are marked in red/green, the reference landmarks after registration are marked in blue. We can see that the landmarks converge (moving from the red spots to the blue spots, to approach the green spots) in accordance with the distortion field. As for the deformed grids, where the grid area expands/shrinks, we observe lighter/darker gray level corresponding to larger/smaller value of the inverse of determinant of Jacobian.

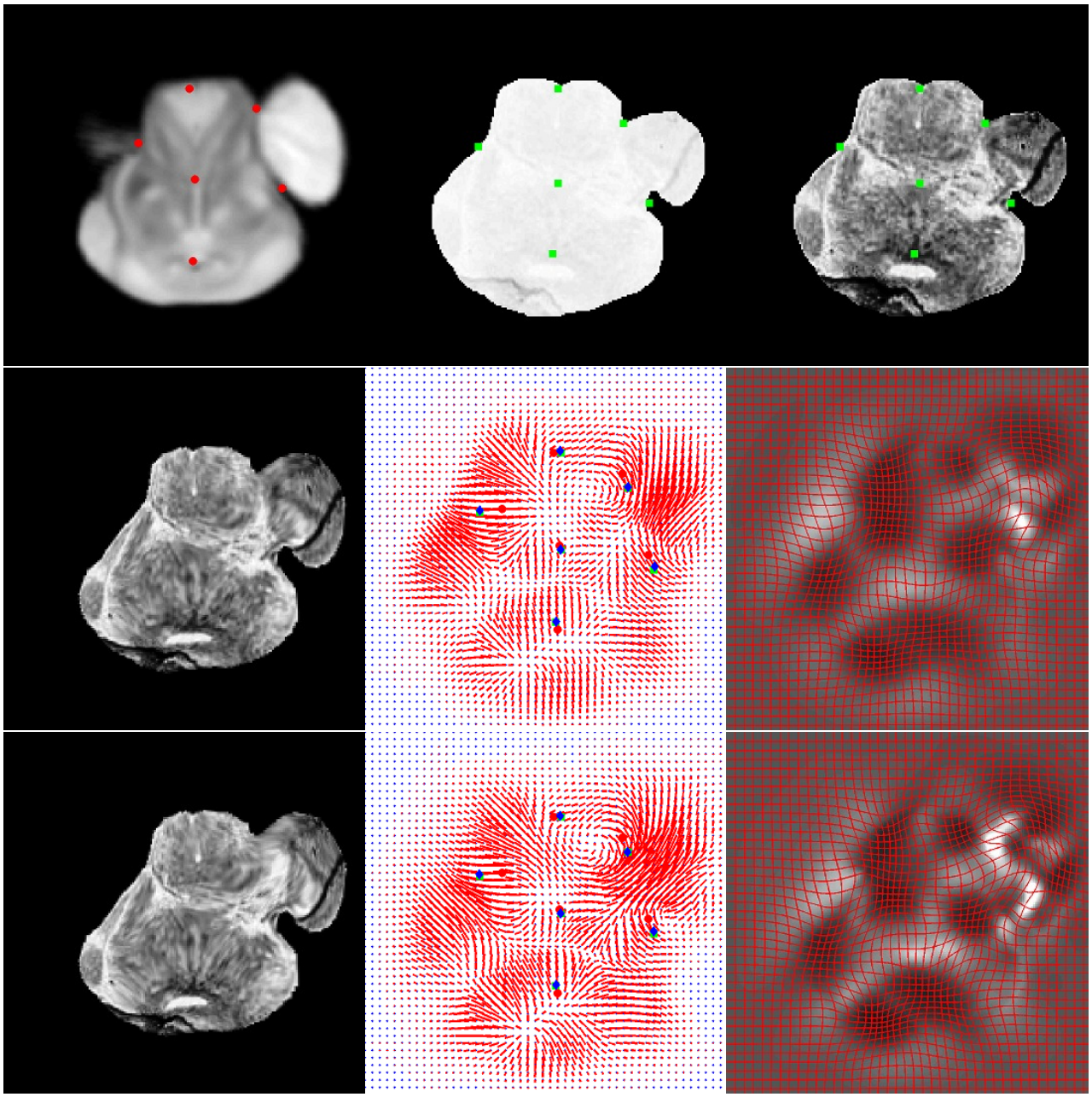

Figure 7. Pair 7: mouse atlas (reference R), gene expression (template T), and gene expression after histogram equalization with specified landmarks (top, left to right); deformed template, deformation field and landmarks transformation, $1/det(\nabla\Phi)$ and deformed grid using BH regularization (middle, left to right), and those using NE regularization (bottom, left to right.)

Quantitative Comparisons of Results Besides the visualization of the registration results shown above, computed quantitative measurements are given in Tables 1-6. Tables 1 and 2 give the landmark distances and the L^2 dissimilarity measures after registration by the two models for the eight pairs of images. The nonlinear elasticity model reaches smaller dissimilarities in overall intensity values and in landmark distance.

We also observe that the nonlinear elasticity model has a slightly larger range of values for the determinant of Jacobian in average but also has a higher average percentage of points where the determinant of Jacobian equals to one. Table 3 gives the range of values for the determinant of Jacobian for the eight pairs of images

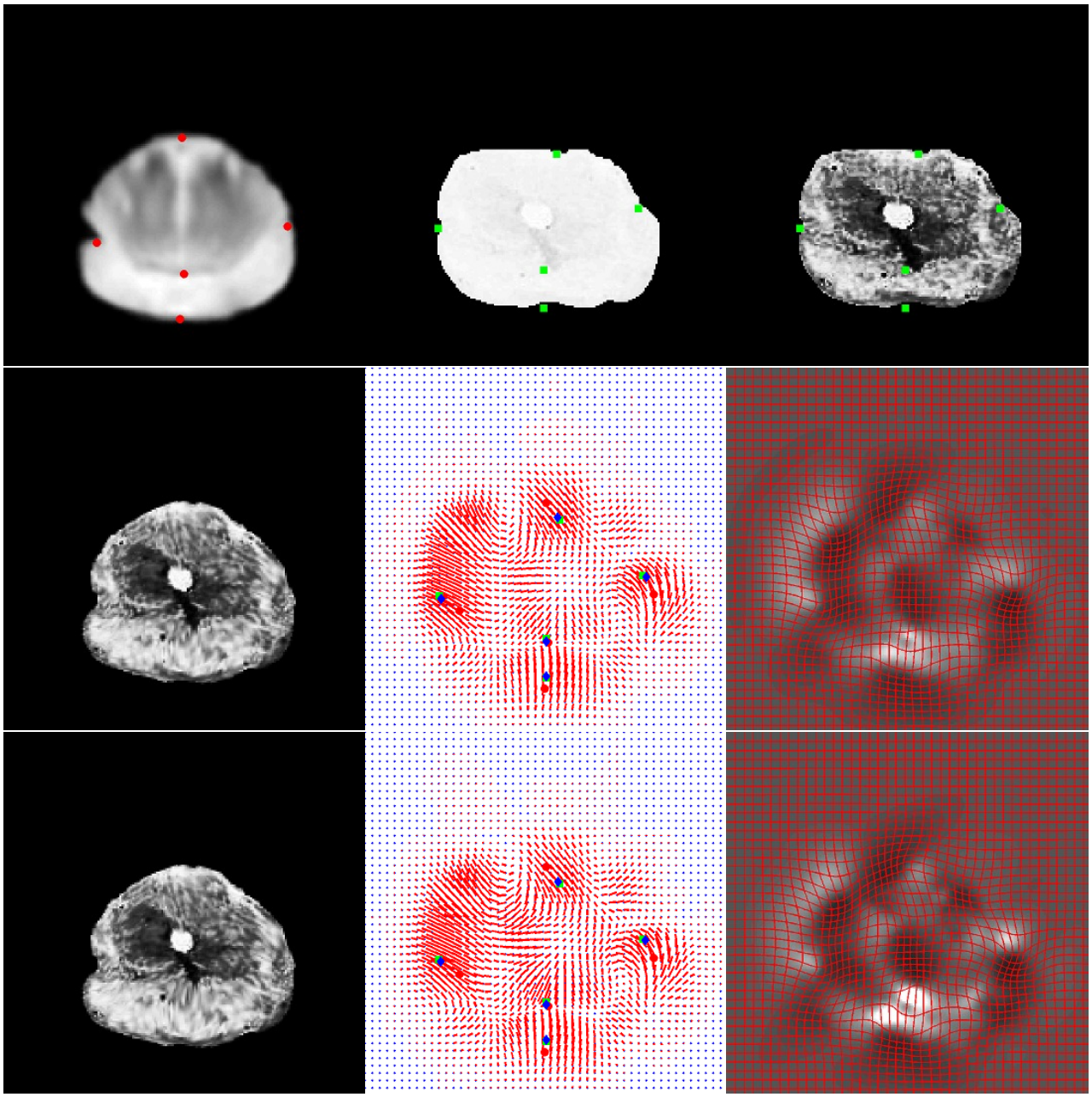

Figure 8. Pair 8: mouse atlas (reference R), gene expression (template T), and gene expression after histogram equalization with specified landmarks (top, left to right); deformed template, deformation field and landmarks transformation, $1/det(\nabla\Phi)$ and deformed grid using BH regularization (middle, left to right), and those using NE regularization (bottom, left to right.)

after registration.

Table 4 gives the percentage of points where the determinant of Jacobian equals to one after registration by the two models for the eight pairs of images. Now we see that the percentages for both models are very close. However, the nonlinear elasticity model renders larger percentages for five out of eight image pairs.

Table 5 gives the iteration numbers for the two models for the eight pairs of images. The number of iterations required by both models are similar given proper choice of parameters; iteration time for the nonlinear elasticity

Table 1. Landmark Distance after Registration

	Pair 1	Pair 2	Pair 3	Pair 4	Pair 5	Pair 6	Pair 7	Pair 8
LMDist(BH)	0.49519	0.42388	0.26758	0.90027	0.70846	0.11232	0.46912	0.71972
LMDist(NE)	0.49282	0.41299	0.26593	0.74304	0.60741	0.10712	0.34660	0.55106

Table 2. Dissimilarity Measure after Registration

	Pair 1	Pair 2	Pair 3	Pair 4	Pair 5	Pair 6	Pair 7	Pair 8
$\|T1-R\|$(BH)	1,942	1,806	1,168	4,130	3,723	1,255	1,266	3,073
$\|T1-R\|$(NE)	1,938	1,790	1,151	4,101	3,693	1,177	1,173	3,058

Table 3. Range of Values for the Determinant of Jacobian

	Pair 1	Pair 2	Pair 3	Pair 4	Pair 5	Pair 6	Pair 7	Pair 8
BH	(.34,3.38)	(.15,2.11)	(.28,1.99)	(.25,2.05)	(.04,1.87)	(.23,2.30)	(.31,2.30)	(.37,2.12)
NE	(.32,3.55)	(.01,3.16)	(.10,2.15)	(.08,2.57)	(.10,2.82)	(.15,2.40)	(.18,3.23)	(.03,2.35)

Table 4. Percentage of Points where the Determinant of Jacobian Equals to One

	Pair 1	Pair 2	Pair 3	Pair 4	Pair 5	Pair 6	Pair 7	Pair 8
BH	%52.74	%52.66	%52.73	%51.08	%57.96	%53.35	%59.75	%52.39
NE	%52.73	%52.44	%54.15	%56.39	%52.05	%53.67	%66.52	%54.29

Table 5. Iteration Numbers

Pair 1	Pair 2	Pair 3	Pair 4	Pair 5	Pair 6	Pair 7	Pair 8
10,000	10,000	10,000	200,000	140,000	4,000	80,000	40,000

Table 6. Parameters

	Pair 1	Pair 2	Pair 3	Pair 4	Pair 5	Pair 6	Pair 7	Pair 8
α	50,000	75,000	50,000	100,000	100,000	75,000	150,000	75,000
γ(BH)	100,000	700,000	300,000	100,000	100,000	700,000	300,000	150,000
β	100,000	120,000	75,000	100,000	75,000	75,000	150,000	100,000
γ(NE)	160,000	190,000	300,000	100,000	700,000	700,000	300,000	150,000

model is about twice as long as that for the biharmonic model (13 to 16 minutes *v.s.* 5 to 7 minutes per 4,000 iterations using Intel(R) Core(TM)2 Duo CPU T7500 @ 2.20GHz processor with code in Matlab); no regridding is needed for both models for gene data to atlas registration given proper choice of parameters.

Finally, Table 6 gives the parameters chosen for the two models for the eight pairs of images: the time step $\triangle t = 1$ and the space discretization $h = 1$ for both models. For the biharmonic model we vary the regularization weighting parameter α and the landmark constraint coefficient γ; for the nonlinear elasticity model, we vary the coefficient β of the approximation matrix $\mathbf{v}$ and γ while fixing $\alpha = 1$, $\lambda = 1$, and $\mu = 1e-2$. The choice of α and β does not vary too much among the tested pairs of images; $\alpha \geq 5e+4$ and $\beta \geq 75e+3$ will give satisfactory results. The choice of γ more or less depends on the total landmark distance before registration; the larger the landmark distance is, the smaller γ should be. Note that an almost constant (or slightly increasing) ratio, γ/α or γ/β, for each image pair can be found; increasing γ in accordance with α or β by the ratio may result in smoother transformation, faster landmark convergence, but slower L^2 similarity convergence.

Mutual Information Comparison of Results Furthermore, we want to evaluate the registration results by comparing how much the deformed template correlates with the reference after being registered by the two

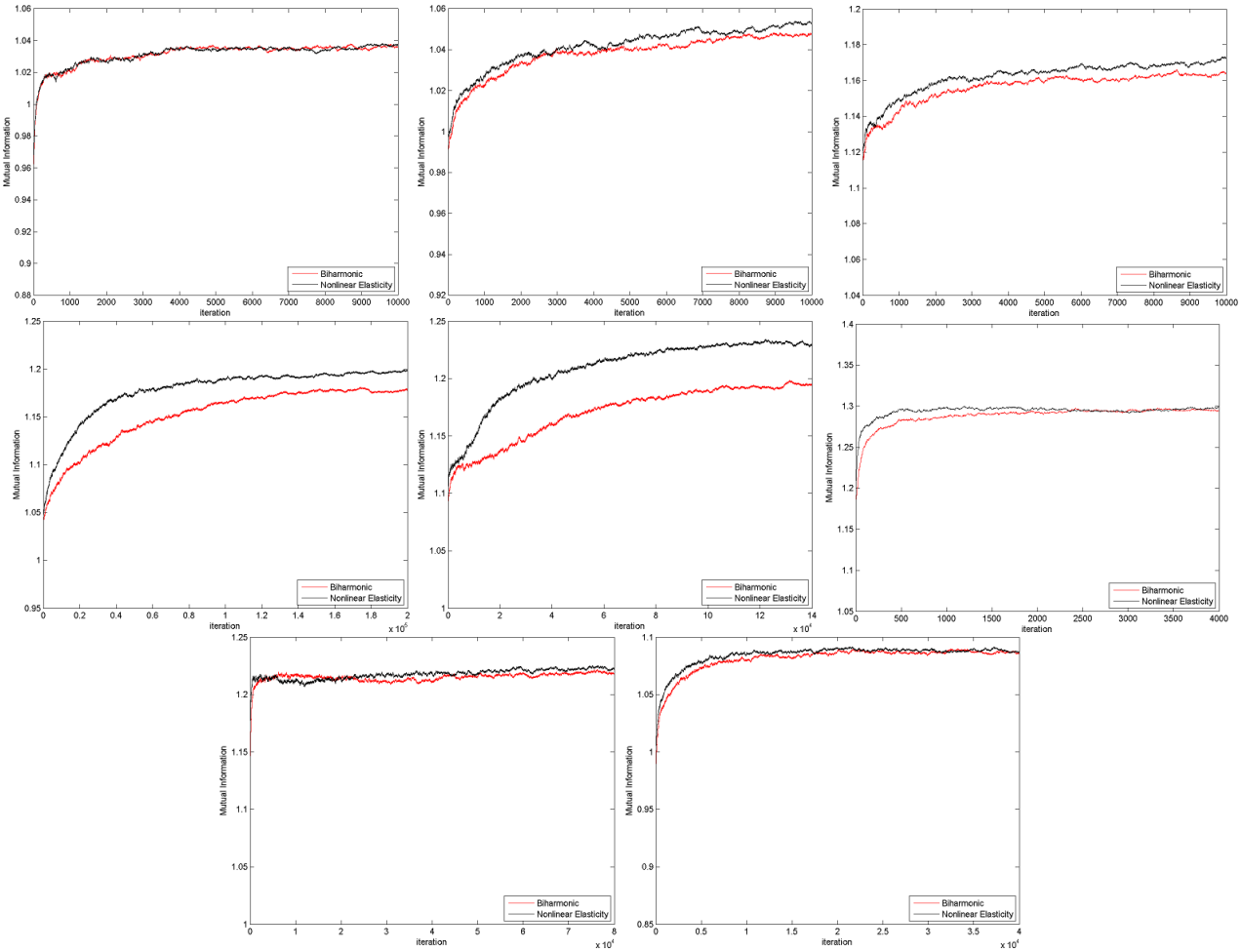

Figure 9. Mutual information increasing with time for all pairs, 4-8, 11, 12, 15 (left to right, top to bottom) using BH regularization (red line), and proposed NE regularization (black line).

models. We use the mutual information, defined for two random variables X and Y in the continuous case by

$$MI(\mathbf{X},\mathbf{Y}) = \int_{\mathbf{Y}}\int_{\mathbf{X}} p(x,y) log \frac{p(x,y)}{p_1(x)p_2(y)}\, dx\, dy,$$

where $p(x,y)$ is the joint probability density function of $\mathbf{X}$ and $\mathbf{Y}$, and $p_1(x)$, $p_2(y)$ are the marginal probability density functions of $\mathbf{X}$ and $\mathbf{Y}$ respectively. The mutual information quantifies the similarity between $\mathbf{X}$ and $\mathbf{Y}$, which in our case are the intensity maps of R and T. Considering that larger mutual information indicates better registration, we see in Fig. 9 (where we visualize the discrete mutual information between intensities of $T(\mathbf{x}+\mathbf{u}(\mathbf{x}))$ and $R(\mathbf{x})$ versus iterations) that the nonlinear elasticity model (MI in black line), is more desirable in this respect. Also, we notice that, although we did not use the mutual information as similarity measure (we have used the simpler L^2 similarity measure, even if T and R are of different modalities), by the proposed algorithms the mutual information between intensities of $T(\mathbf{x}+\mathbf{u}(\mathbf{x}))$ and $R(\mathbf{x})$ increases over iterations. Moreover, as mentioned above, the increase is faster for the nonlinear elasticity smoother, most of the time.

4. CONCLUSION AND FUTURE WORK

We presented variational registration models for obtaining smooth deformations between two dimensional slices of mouse atlas and gene expression data, in the presence of landmarks. We proposed a nonlinear elastic regularization with an implementation that removes the nonlinearity in the derivatives and compared it with the

biharmonic (curvature) model. Extensive experimental results and assessment showed that the biharmonic model and the nonlinear elasticity model both render relatively large deformations with no regridding; however, the nonlinear elasticity model renders higher mutual information over time and better landmark points matching.

ACKNOWLEDGMENTS

The authors would like to thank Alex Bui, Jan Modersitzki, Hemant Tagare, Roger Temam and Igor Yanovsky for their useful suggestions about registration and visualization. This work was funded by the National Institutes of Health through the NIH Roadmap for Medical Research, Grant U54 RR021813 entitled Center for Computational Biology (CCB).

REFERENCES

[1] Modersitzki, J., [*Numerical Methods for Image Registration*], Oxford University Press (2004).
[2] Faugeras, O. and Hermosillo, G., "Well-posedness of two nonrigid multimodal image registration methods," *SIAM Appl. Maths.* **64**(5), 1550–1587 (2004).
[3] Christensen, G., Rabbitt, R., and Miller, M., "Deformable templates using large deformation kinematics," *IEEE TIP* **5**(10), 1435–1447 (1996).
[4] Beg, F., Miller, M., Trouvé, A., and Younes, L., "Computing large deformation metric mappings via geodesic flows of diffeomorphisms," *IJCV* **61**(2), 139–157 (2005).
[5] Miller, M., Trouvé, A., and Younes, L., "On the metrics and Euler-Lagrange equations of computational anatomy," *Annu. Rev. B. Eng* **4**, 375–405 (2002).
[6] Yanovsky, I., Osher, S., Thompson, P., and Leow, A., "Log-unbiased large-deformation image registration," *VISAPP* **1**, 272–279 (2007).
[7] Yanovsky, I., Thompson, P., Osher, S., and Leow, A., "Topology preserving log-unbiased nonlinear image registration: Theory and implementation," *CVPR* , 1–8 (2007).
[8] Rabbitt, R. D., Weiss, J. A., Christensen, G. E., and Miller, M. I., "Mapping of hyperelastic deformable templates using the finite element method," in [*Proceedings SPIE*], **2573**, 252–265 (1995).
[9] Peckar, W., Schnörr, C., Rohr, K., and Stiehl, H., "Parameter-free elastic deformation approach for 2D and 3D registration using prescribed displacements," *JMIV* **10**(2), 143–162 (1999).
[10] Droske, M. and Rumpf, M., "A variational approach to non-rigid morphological registration," *SIAM Appl. Math.* **64**(2), 668–687 (2004).
[11] Johnson, H. and Christensen, G., "Consistent landmark and intensity-based image registration," *IEEE TMI* **21**(5), 450–461 (2002).
[12] Sorzano, C., Thévenaz, P., and Unser, M., "Elastic registration of biological images using vector-spline regularization," *IEEE T. Biom. Eng.* **52**(4), 652–663 (2005).
[13] Marrero, P. N., "A numerical method for detecting singular minimizers of multidimensional problems in nonlinear elasticity," *Numerische Mathematik* **58**(1), 135–144 (1990).
[14] LeGuyader, C. and Vese, L., "A combined segmentation and registration framework with a nonlinear elasticity smoother," *UCLA CAM Report 08-16* (March 2008).
[15] Lin, T., Lee, E.-F., Dinov, I., LeGuyader, C., Thompson, P., Toga, A., and Vese, L., "A landmark-based nonlinear elasticity model for mouse atlas registration," in [*ISBI 2008. 5th IEEE International Symposium on Biomedical Imaging: From Nano to Macro*], 788 – 791 (2008).
[16] MacKenzie-Graham, A., Lee, E.-F., Dinov, I., Yuan, H., Jacobs, R., and Toga, A., "Multimodal, multidimensional models of mouse brain," *Epilepsia* **48, Supplement 4**, 75–81(7) (2007).
[17] Lee, E.-F., Jacobs, R., Dinov, I., Leow, A., and Toga, A., "Standard atlas space for c57bl/6j neonatal mouse brain," *Anat. Embryol (Berl).* **210**(4), 245–263 (2005).
[18] Broit, C., *Optimal Registration of Deformed Images*, PhD thesis, Computer and Information Science, University of Pensylvania (1981).
[19] Ciarlet, P.-G., [*Elasticité Tridimensionnelle*], Masson (1985).
[20] Temam, R. and Miranville, A., [*Mathematical Modeling in Continuum Mechanics*], Cambridge (2005).